Published in final edited form as:

Mol Cancer Ther. 2007 June ; 6(6): 1701–1708. doi:10.1158/1535-7163.MCT-07-0121.

Detection of myeloma in skeleton of mice by whole-body optical fluorescence imaging

Babatunde O. Oyajobi[1,2,3], **Steve Muñoz**[1], **Rami Kakonen**[1], **Paul J. Williams**[1], **Anjana Gupta**[1], **Christi L. Wideman**[1], **Beryl Story**[1], **Barry Grubbs**[1], **Allison Armstrong**[5], **William C. Dougall**[5], **I. Ross Garrett**[4], and **Gregory R. Mundy**[1,2,3]

[1]Department of Molecular Medicine, University of Texas Health Science Center at San Antonio

[2]Molecular Therapeutics Division, Institute for Drug Development

[3]San Antonio Cancer Institute

[4]OsteoScreen Ltd., San Antonio, Texas

[5]Cancer Biology, Amgen Washington, Seattle, Washington

Abstract

Development of new therapies for myeloma has been hindered by the lack of suitable preclinical animal models of the disease in which widespread tumor foci in the skeleton can be detected reliably. Traditional means of detecting skeletal tumor infiltration such as histopathology are cumbersome and labor-intensive and do not allow temporal monitoring of tumor progression or regression in response to therapy. To resolve this problem, we modified the Radl 5TGM1 model of myeloma bone disease such that fluorescent myeloma tumors can be optically imaged *in situ*. Here, we show that murine myeloma 5TGM1 tumor cells, engineered to express enhanced green fluorescent protein (eGFP; 5TGM1-eGFP cells), can be imaged in a temporal fashion using a fluorescence illuminator and a charge-coupled device camera in skeletons of live C57BL/KaLwRij mice. High-resolution, whole-body images of tumor-bearing mice revealed that myeloma cells homed almost exclusively to the skeleton, with multiple focal tumor foci in the axial skeleton, consistent with myeloma tumor distribution in humans. Finally, the tested antitumor treatment effect of Velcade (bortezomib), a proteasome inhibitor used clinically in myeloma, was readily detected by GFP imaging, suggesting the power of the technique in combination with the Radl 5TGM1-eGFP model for rapid preclinical assessment and sensitive monitoring of novel and potential therapeutics. Whole-body GFP imaging is practical, convenient, inexpensive, and rapid, and these advantages should enable a high throughput when evaluating *in vivo* efficacy of new potential antimyeloma therapeutics and assessing response to treatment.

Requests for reprints: Babatunde O. Oyajobi, Department of Cellular and Structural Biology (MSC 7762), University of Texas Health Science Center at San Antonio, 7703 Floyd Curl Drive, San Antonio, TX 78229-3900., Phone: 210-567-0925; Fax: 1-210-567-3803., oyajobi@uthscsa.edu.

Note: Present address for B.O. Oyajobi: Department of Cellular & Structural Biology, University of Texas Health Science Center at San Antonio, San Antonio, TX 78229-3900; Present address for R. Kakonen: Pharmatest Services Ltd., 20520 Turku, Finland; Present address for G.R. Mundy: Department of Medicine, Vanderbilt Center for Bone Biology, Vanderbilt, University Medical Center, Nashville, TN 37232-0575.

Introduction

Multiple myeloma is the second most common adult hematologic malignancy and affects 19,000 patients in the United States annually (1). It is characterized by a unique form of progressive bone destruction (2, 3) and, despite the increasing number of available therapeutic strategies (4), morbidity and mortality rates have remained high in these patients (1). This lack of progress has been due, in part, to the lack of good preclinical models for testing candidate compounds or drugs. Unlike solid tumors in humans with distinct primary sites, the malignant plasma cells in multiple myeloma are often diffusely spread throughout the bone marrow (5). The Radl 5TGM1/5T33 and 5T2 myeloma models have been shown to most faithfully replicate the human disease (6–15). However, tumor progression in these models is usually followed with serum titers of the monoclonal paraprotein, which are prone to false negatives. A reliable whole-body imaging technique is necessary, therefore, to accurately assess the extent and activity of these diffuse tumors and for preclinical drug evaluation in these models. Recently, visualization of cancer cells in the skeleton of mouse models of human tumors has become possible by improved imaging technologies and the use of cells stably expressing the bioluminescent jellyfish *Aequorea victoria* protein [green fluorescent protein (GFP)] or its variants such as enhanced GFP (eGFP). GFP imaging is reportedly more sensitive and rapid than traditional histopathology and other imaging modalities (16, 17). We hypothesized that GFP imaging would facilitate a more rapid preclinical evaluation of antitumor efficacy of novel agents than hitherto possible. Here, we report the generation of murine myeloma 5TGM1 cells genetically engineered to stably express eGFP (5TGM1-eGFP cells) and inoculated into syngeneic C57BL mice to produce genetically fluorescent tumors throughout the mouse skeleton. As proof-of-principle, we show the utility of GFP imaging in rapid evaluation of antitumor efficacy in 5TGM1-eGFP myeloma–bearing mice treated with bortezomib (Velcade; PS-341), a proteasome inhibitor with known antitumor effects in myeloma patients (18). This Radl 5TGM1-eGFP model has the potential to advance the development and translation of novel antimyeloma strategies and agents.

Materials and Methods

Murine 5TGM1-eGFP Myeloma Model

The establishment of the 5TGM1 myeloma cell line from the parent 5T33 myeloma (7, 8) and the protocol for its long-term maintenance in culture have been reported (7–9). eGFP (Clontech) was subcloned into the LZRS-pBMNZ vector and production of infectious retroviral particles was done in 293-E.Phoenix packaging cells as described (19). 5TGM1 cells were transduced with these viruses, and cells stably expressing eGFP were sorted by single-color flow cytometry on a Becton Dickinson FACStar Plus flow cytometer equipped with an automatic cell deposition unit (University of Texas Health Science Center at San Antonio Institutional Flow Cytometry Core) and initially expanded as a pool. Several high eGFP-expressing 5TGM1 clones were subsequently isolated following single-cell cloning by fluorescence-activated cell sorting of the brightest 1% fluorescent cells within the pool. Of these, one high-expressing clone, designated 5TGM1-eGFP H1.1+, was selected for further characterization *in vitro* and *in vivo*.

Animal studies were conducted using 6- to 9-week-old female C57BL/KaLwRijHsd mice (Harlan) in accordance with the NIH Guide for the Care and Use of Laboratory Animals. Myeloma lesions were induced in mice by i.v. inoculation of 10^6 viable 5TGM1-eGFP H1.1+ cells or parental 5TGM1 cells through tail veins. Viability was routinely checked by trypan blue dye exclusion test before inoculation and was always ≥96%. Establishment of myeloma tumor in inoculated mice was followed by assaying 5TGM1-specific immunoglobulin G2bκ (IgG2κ) monoclonal paraprotein in sera prepared from whole blood obtained by retro-orbital sinus bleed, under light methoxy-flurane-induced anesthesia, and stored frozen for determination of IgG2bκ titers. Mouse IgG2bκ levels were assayed by a specific in-house ELISA, with no species cross-reactivity or cross-reactivity to other mouse immunoglobulins, as described (8).

Real-time Optical Imaging of Fluorescence inMice

Following administration of light inhalation anesthetic (methoxyflurane; Medical Developments Australia), tumor-bearing mice were completely depilated using Nair hair depilatory lotion before imaging because hair can significantly scatter light from underlying structures, thus quenching fluorescence. Selective excitation of GFP in intact live animals was achieved using an Illumatools fiber-optic fluorescence lighting system (Epi model LT-9500; Lightools Research, Inc.) with a 470/40 nm band-pass filter and a dichroic mirror. Emitted fluorescence was collected through a long-pass filter at 515 nm with a MagnaFire SP cooled color methoxy (Optronics) with an 11- to 48-mm zoom lens, with exposure times of up to 60 s. Routinely, after sacrifice, whole skeletons and visceral organs (spleens, livers, kidneys, gonads, brains, lungs, and hearts) were removed and also imaged for fluorescent tumor foci. High-resolution images (1,300 × 1,030 pixels) were captured directly on a PC and adjusted for gamma contrast and brightness using ImagePro and Lucis 2.0 and analyzed using MetaMorph software (Universal Imaging Corp.). For quantification of fluorescence from serial images obtained from each individual mouse, the person doing the analysis selected upper and lower limits on the final image. This allows the MetaMorph software to automatically set an inclusive threshold. All pixels within this range were then selected automatically on every image, the area was overlaid in red, and an arbitrary fluorescence unit was generated. All analyses were carried out by the same blinded individual.

Bone Histologic and Cytochemical Analyses

Animals were sacrificed by cervical dislocation under ketamine-induced anesthesia, and the skeleton and soft organs were removed and rapidly imaged for fluorescent tumor foci before significant effects from postmortem changes occurred. All tissues were then fixed in 10% formalin for 48 h and the bones subsequently decalcified in 14% EDTA for 1 to 2 weeks. Fixed soft organs, embedded in paraffin, were sectioned at 5 μm and stained with H&E. Serial bone sections were stained with H&E and for tartrate-resistant acid phosphatase activity, a marker of osteoclasts in mouse bone *in vivo*. Fixed and decalcified bones, also embedded in paraffin, were sectioned along the midsagittal plane at 7 μm. Serial bone sections were stained with H&E and for tartrate-resistant acid phosphatase activity (8, 9).

Optical Imaging to Assess Drug Efficacy: Effect of Velcade Administration

To further assess the feasibility of using the 5TGM1-eGFP model for routine preclinical assessment of antitumor drug efficacy, groups of C57BL/KaLwRijHsd mice were treated with or without Velcade (bortezomib, PS-341). Velcade (Millennium Pharmaceuticals) was diluted in sterile PBS per manufacturer's instructions. Age- and sex-matched mice were i.v. inoculated with 5TGM1-eGFP cells and then randomized into groups ($n = 8$ per group) to receive varying doses of the drug (0.1, 0.5, 1, and 3 mg/kg of body weight) or vehicle i.p. thrice a week for 4 weeks. Age- and sex-matched non–umor-bearing mice ($n \geq 4$/group) treated with or without Velcade (3 mg/kg) served as controls. Body weights of animals were also determined at baseline and weekly thereafter. At the end of 4 weeks, whole mice were imaged and, immediately after sacrifice, skeletons and visceral organs (spleens, livers, kidneys, gonads, brains, lungs, and hearts) were dissected out and also imaged for fluorescent tumor foci to assess tumor burden.

Results and Discussion

Of the available preclinical models of multiple myeloma, the murine 5T model originally described by Radl et al. (6) is the most promising in terms of faithfully replicating the disease as in humans (6; reviewed in ref. 5). Myelomas that arose spontaneously in aged, in-bred C57BL/KaL-wRijHsd mice were propagated by serial transplantation into young immunocompetent syngeneic recipients (6). The series of tumors, designated 5T myelomas, share a number of clinical, histologic, cytogenetic, and molecular genetic features with the human disease (6–15). When inoculated i.v. into syngeneic C57BL/KaLwRij mice, 5T myeloma tumor cells home almost exclusively to the bone marrow and infrequently to the spleen. Additionally, bone destruction is evident around tumor foci and the lytic lesions can be visualized by plain radiography, with increased osteoclastic activity documented by bone histomorphometry (7, 8, 13, 14). The original Radl myeloma model was established using whole marrow transplants from mice bearing the 5T33 myeloma (6). More recently, we established a stroma-independent subclone from a cell line originally derived from the IgG2bκ-secreting 5T33 myeloma, which gives identical results when inoculated into appropriate hosts (7–9). This allows inoculation of precise numbers of myeloma cells into mice. Because we can monitor development of radiographically visible lytic lesions temporally and accurately predict the time to development of paraplegia and death, the 5TGM1/5T33 myeloma model has proved a convenient model for preclinical evaluation of candidate compounds/drugs (8, 9, 15). However, even in the Radl model, there has been no appropriate way of reliably following overall tumor burden except for serum titers of the monoclonal paraprotein titers. Optical imaging of GFP-expressing cancer cells offers a means of visualizing tumors *in situ* in whole intact animals (16, 17), and we reasoned that combining the 5TGM1 myeloma model with GFP imaging would facilitate accurate monitoring of myeloma tumors disseminated throughout the skeleton. This capability is especially important in settings where the model is being used to predict efficacy of antitumor agents, as there is a marked decrease in emitted fluorescence observed following death induction in cells expressing eGFP (20).

In this study, we developed a mouse model of myeloma bone disease based on the 5TGM1 cell line genetically engineered to stably express eGFP. One high eGFP-expressing clone, 5TGM1eGFP H1.1+ (Fig. 1A and B), isolated from 5TGM1 cells retrovirally transduced with a bicistronic vector encoding eGFP, has been further characterized *in vitro* and *in vivo*. 5TGM1-eGFP H1.1+ cells have been maintained in culture without loss or diminution in GFP expression as determined by single-color fluorescence-activated cell sorting analysis. Similarly, GFP expression in 5TGM1-eGFP H1.1+ passaged repeatedly in syngeneic C57BL/KaLwRij mice has remained stable (Fig. 1B). There was no significant difference in the *in vitro* growth of 5TGM1-eGFP H1.1+ cells compared with parental 5TGM1 cells (Fig. 1C) or the monoclonal paraprotein production (data not shown). Using an illuminator and a thermoelectrically cooled CCD camera, genetically fluorescent myeloma tumors growing *in situ* in the skeleton were visualized on high-resolution, whole-body optical images of live 5TGM1-eGFP tumor–bearing mice (Fig. 2A–E). Consistent with our previous observation that tumor "take" requires at least 10^5 5TGM1 cells, fluorescent tumors could be visualized on images of mice inoculated with 10^5 5TGM1-eGFP–expressing cells, and no tumors were visible in mice inoculated with a log less cells even after 8 weeks (data not shown). Examination of freshly isolated tissues from these tumor-bearing mice revealed that the eGFP-expressing myeloma cells have a predilection for the skeleton in all mice, with multifocal fluorescent lesions particularly pronounced in the axial skeleton (skull, pelvis, lumbar and thoracic vertebrae, ribs, scapula, sternum, and clavicle). These lesions were also evident in the metaphyseal regions of long bones, especially femorae and humeri (Fig. 2B–D), also consistent with typical tumor distribution in myeloma patients. We did time-course studies examining freshly isolated skeleton of mice inoculated with tumor cells. Consistent with the previous results, we found that the earliest time that fluorescent tumor foci were detectable was between 10 and 14 days post tumor inoculation, and this was always in the scapula or calvaria. Although the significance of these findings is presently unclear, it is likely due to differences in the marrow in bones that develop by membranous ossification versus endochondral ossification. Smaller extramedullary tumor foci were infrequently detectable in spleen and ovaries but not in livers and other visceral organs of tumor-bearing mice (Fig. 2F). This is consistent with previous studies in which we have shown splenic involvement in this myeloma model (8, 9), presumably because the spleen is a surrogate hematopoietic organ in the mouse. Because imaging fluorescence emitted *in vivo* by GFP-expressing cells is inherently noninvasive (16, 17, 21), we next examined the feasibility of monitoring tumor progression in intact 5TGM1-eGFP tumor–bearing mice. We found that the same tumor foci in a particular bone in live intact mouse could be imaged repeatedly over time without any apparent adverse effects, and a representative example is shown of tumors in the skull (Fig. 3A). We further showed that the emitted fluorescence could be semiquantified by computerized image analysis to illustrate a time-dependent increase in tumor growth within individual bones (Fig. 3B).

The major criteria necessary for a good *in vivo* technique for imaging tumors are that there are few or no false positives or false negatives. We confirmed by histology in all cases that areas of bones that are fluorescent on imaging indeed represent tumor foci (Fig. 4A, B, D, and E), representing a high level of GFP imaging sensitivity. Moreover, we also confirmed by enzyme cytochemistry for tartrate-resistant acid phosphatase activity (a marker of

osteoclasts) that these tumor foci are associated with increased osteoclastic activity (Fig. 4C and F). The calvariae and humeri are representative parts of the skeleton that are not typically included in histomorphometric analyses of myeloma-bearing mice, but nevertheless may be completely infiltrated with tumor. In extensive histopathologic examinations, we have thus far detected no false negatives (i.e., tumor foci that were not detected prior by imaging) either in the skeleton or visceral organs. Apart from the nails that autofluoresce, routine examination of non–tumor-bearing mice reveal no false positives, making this imaging modality not only very sensitive but also highly specific.

There are several disadvantages of the traditional means of assessing myeloma tumor burden and bone disease in available preclinical mouse models of myeloma. Serum monoclonal paraprotein titers are prone to false negatives because of the relatively long half-life of immunoglobulins in the circulation (~3 weeks); thus, there may be no discernable titer reductions even when potentially efficacious agents are being tested. With regards to myeloma-induced osteolytic bone disease, the gold standard for assessing this disease in mouse models is histology and bone histomorphometry. However, although these techniques are extremely useful in assessing tumor involvement in predetermined skeletal sites, histomorphometric analyses are in most cases restricted to the long bones of the hind limbs and lumbar vertebrae. As shown in Fig. 2, several high-risk disease sites such as calvariae, iliac crests, and scapulae are not routinely evaluated for the presence of focal or diffuse bone involvement with these methods. This inherent localized and spatially restrictive nature of histomorphometry does not permit accurate assessment of tumor burden throughout the skeleton and can readily lead to false positives during preclinical evaluation of novel therapies. Temporal monitoring of tumor progression is also not feasible with bone histomorphometry. All of these factors are further compounded by the cumbersome, time-consuming, and expensive nature of histomorphometry, making it unsuitable for use as a whole-body screening technique. Consistent with other reports involving GFP-expressing breast cancer cells (17), we found tracking of GFP-expressing myeloma cells engrafted in the mouse skeleton to be clearly superior in sensitivity to plain radiography in detecting evidence of bone involvement. As is sometimes the case with patients, radiographs of myeloma-bearing mice can significantly underestimate the extent and magnitude of bone and bone marrow involvement. We found that in several instances, fluorescent tumor foci were detectable in 5TGM1-eGFP tumor–bearing mice as early as 2 weeks post tumor inoculation. At this point in the course of the disease, all the radiographs taken concurrently were negative and devoid of any radiolucent lytic lesions (data not shown). Thus, the capability to carry out whole-body GFP-based optical imaging in the 5TGM1 model presents many advantages over current methods of monitoring tumor progression and bone disease.

To date, unlike with subcutaneous myeloma xenografts, most outcome studies in disseminated models of myeloma growth mouse tumor models rely on histologic and invasive study end points. Tumor growth can be readily assessed noninvasively in patients using high-resolution *in vivo* imaging techniques including radionuclide imaging, such as positron emission tomography and single photon emission tomography, magnetic resonance imaging, and computed tomographic scanning. Although, in recent years, advances have

been made to generate micro-positron emission tomography, micro-single-photon emission computed tomography, and micro-computed tomography suitable for rodents, the use of these for most tumor models including mouse models of myeloma have yet to be validated. Even where dedicated rodent scanners are available, they share disadvantages in terms of high costs, technical expertise required, and overall animal throughput for analyses. Moreover, the above techniques are not readily adaptable for preclinical drug efficacy screens. We reasoned that GFP imaging would be an alternative, rapid, and relatively inexpensive means of assessing antitumor drug efficacy. To further validate this notion, we did a proof-of-principle experiment in which Velcade, the first-in-class proteasome inhibitor to be approved for clinical use, was predicted to significantly inhibit tumor growth *in vivo* in the 5TGM1-eGFP model. Velcade has consistently been shown to have a dramatic antimyeloma effect in patients, and we found that the drug also rapidly induces cell death in cultures of 5TGM1 cells (with an IC_{50} of 1–5 nmol/L; data not shown). In mice inoculated with 5TGM1-eGFP cells, untreated tumor growth was readily detected and observed over time by serial fluorescence imaging. Mice treated with Velcade had significantly decreased skeletal tumor burden, as determined by fluorescence imaging, and this effect of the drug was clearly dose dependent (Table 1; Fig. 5) with significant abrogation of tumor or almost complete absence of tumor in the skeleton at the two highest doses tested. Velcade was equally effective in eradicating tumor from spleen and other soft tissues (Table 1). This effect of Velcade was discernable immediately after the experiment was terminated, in contrast to previous techniques for assessing antitumor efficacy such as histology wherein unequivocal evidence of an antitumor effect of a compound may not be available for several weeks after the end of an experiment. Thus, the speed of fluorescence imaging can potentially increase experimental throughput significantly. To further support the validity of GFP imaging for assessing tumor burden, we determined the levels of the monoclonal IgG2bκ paraprotein in sera obtained from experimental animals just before sacrifice. There was concordance between the dose-dependent effects of Velcade to reduce tumor load observable with GFP imaging and assessed by IgG2bκ titers (data not shown). Together, these data show the utility of this model and of fluorescence imaging for rapid screening for drug efficacy and assessment of response to treatment.

There have been previous attempts at fluorescence tagging of myeloma cells to establish mouse models. Mitsiades et al. (21) inoculated human myeloma RPMI 8226 cells expressing GFP into irradiated severe combined immunodeficient (SCID)/nonobese diabetic mice and found that whole-body imaging antemortem or immediately postmortem, as presented in this report, was not very successful. Although myeloma can also present in extramedullary sites such as visceral organs in humans, clinical presentation as subcutaneous masses is extremely rare. However, ~67% of the mice bearing RPMI 8226 xenografts also had multiple subcutaneous plasmacytomas. This is not only inconsistent with the typical clinical course of human multiple myeloma but it also makes the relevance of the SCID/RPMI 8226-GFP model uncertain at best. Bioluminescence imaging has also been used for tracking tumor development *in vivo*. However, luminescence-based imaging requires systemic injection of an enzyme substrate, and signal intensity depends on the availability of the substrate within living cells in intact organs. The biodistribution and clearance rates of the substrate are therefore directly related to optimal imaging times and signal intensities. However, these

factors, which may vary considerably depending on extent of tumor in each organ, ultimately determine the sensitivity of detection and predictability of a model. Pharmacokinetic and pharmacodynamic properties as well as costs of the substrate are not issues with GFP imaging; moreover, GFP imaging avoids the effect of additional stress from injections in tumor-bearing animals that may already be moribund. Thus, overall, GFP imaging is more practical and less expensive in the long term.

In summary, imaging of fluorescent tumors *in situ* in mice is a more sensitive and effective means of assessing disease progression and tumor load in the 5T myeloma model than previously available techniques. One powerful feature of this imaging modality for the study of myeloma is the ability to externally and noninvasively image the fluorescence emitted by the GFP-expressing tumor cells in real time. Importantly, visualization of emitted fluorescence requires no preparative procedures, substrates, or contrast agents, and it is convenient and relatively inexpensive. Moreover, 5TGM1-eGFP myeloma cells could be used to develop high-throughput GFP-based microplate cytotoxicity screens for evaluation of novel anticancer agents, as shown for other eGFP-expressing tumor-derived cells (20). *In vivo* efficacy of positive “hits” could then be rapidly determined in mice inoculated with the same 5TGM1-eGFP cells as we have shown in this report. The 5TGM1 model has already proved to be predictive of efficacy in preclinical drug testing (8) and these new capabilities suggest the potential utility of the Radl 5TGM1 model in large-scale anticancer drug screening. This should accelerate discovery, evaluation, and development of novel therapies for myeloma (4).

Acknowledgments

We thank Dr. Garry Nolan for the gift of retroviral vector (Stanford, CA) and Charles Thomas (Flow Cytometry Core, University of Texas Health Science Center at San Antonio) for excellent technical assistance.

Grant support: NIH/National Cancer Institute grants KO1 CA104180 (B.O. Oyajobi) and PO1 CA40035 (G.R. Mundy) and an unrestricted research grant from Immunex Corporation (now Amgen Washington; to B.O. Oyajobi). The University of Texas Health Science Center at San Antonio flow cytometry facility is supported by Cancer Center Grant P30 CA054174 to the San Antonio Cancer Institute.

References

1. Jemal A, Siegel R, Ward E, et al. Cancer statistics, 2007. CA Cancer J Clin. 2007; 57:43–66. [PubMed: 17237035]
2. Oyajobi, BO.; Mundy, GR. Pathophysiology of myeloma bone disease. In: Garhton, G.; Durie, BGM.; Samson, DS., editors. Multiple myeloma and related diseases. 2nd ed.. London: Arnold; 2004. p. 74-78.
3. Kyle RA, Rajkumar SV. Multiple myeloma. N Eng J Med. 2004; 351:1860–1873.
4. Cavo M, Baccarani M. Changing landscape of myeloma therapy. N Eng J Med. 2006; 354:1076–1078.
5. Angtuaco EJ, Fassas AB, Walker R, Sethi R, Barlogie B. Multiple myeloma: clinical review and diagnostic imaging. Radiology. 2004; 231:11–23. [PubMed: 14990813]
6. Radl J, Croese JW, Zurcher C, van den Enden-Vieveen MM, de Leeuw AM. Animal model of human disease: multiple myeloma. Am J Pathol. 1998; 132:593–597. [PubMed: 3414786]
7. Garrett IR, Dallas S, Radl J, Mundy GR. A murine model of myeloma bone disease. Bone. 1997; 20:515–520. [PubMed: 9177864]

8. Dallas SL, Garrett IR, Oyajobi BO, et al. Ibandronate reduces osteolytic lesions but not tumor burden in a murine model of myeloma bone disease. Blood. 1999; 93:1697–1706. [PubMed: 10029599]

9. Oyajobi BO, Franchin G, Williams PJ, et al. Dual effects of macrophage inflammatory protein-1α on osteolysis and tumor burden in the murine 5TGM1 model of myeloma bone disease. Blood. 2003; 102:311–319. [PubMed: 12649140]

10. van den Akker TW, Radl J, Franken-Postma E, Hagemeijer A. Cytogenetic findings in mouse multiple myeloma and Waldenstrom's macroglobulinaemia. Cancer Genet Cytogenet. 1996; 86:156–161. [PubMed: 8603345]

11. Zhu D, Van Arkel C, King CA, et al. Immunoglobulin Vh gene sequence analysis of spontaneous murine immunoglobulin-secreting B-cell tumours with clinical features of human disease. Immunology. 1998; 93:162–170. [PubMed: 9616364]

12. Bakkus MH, Asosingh K, Vanderkerken K, et al. Myeloma isotypeswitch variants in the murine 5T myeloma model: evidence that myeloma IgM and IgA expressing subclones can originate from the IgG expressing tumour. Leukemia. 2001; 15:1127–1132. [PubMed: 11455984]

13. Vanderkerken K, Goes E, De Raeve H, Radl J, Van Camp B. Follow-up of bone lesions in an experimental multiple myeloma mouse model: description of an *in vivo* technique using radiography dedicated for mammography. Br J Cancer. 1996; 73:1463–1465. [PubMed: 8664113]

14. Vanderkerken K, De Raeve H, Goes E, et al. Organ involvement and phenotypic adhesion profile of 5T2 and 5T33 myeloma cells in the C57BL/KaLwRij mouse. Br J Cancer. 1997; 76:451–460. [PubMed: 9275021]

15. Mittelman M, Neumann D, Peled A, Kanter P, Haran-Ghera N. Erythropoietin induces tumor regression and antitumor immune responses in murine myeloma models. Proc Natl Acad Sci U S A. 2001; 98:5181–5186. [PubMed: 11309490]

16. Yang M, Baranov E, Jiang P, et al. Whole-body optical imaging of green fluorescent protein-expressing tumors and metastases. Proc Natl Acad Sci U S A. 2000; 97:1206–1211. [PubMed: 10655509]

17. Peyruchaud O, Winding B, Pecheur I, Serre CM, Delmas P, Clezardin P. Early detection of bone metastases in a murine model using fluorescent human breast cancer cells: application to the use of the bisphosphonate zoledronic acid in the treatment of osteolytic lesions. J Bone Miner Res. 2001; 16:2027–2034. [PubMed: 11697798]

18. Caravita T, de Fabritiis P, Palumbo A, Amadori S, Boccadoro M. Bortezomib: efficacy comparisons in solid tumors and hematologic malignancies. Nat Clin Pract Oncol. 2006; 3:374–387. [PubMed: 16826218]

19. Kinsella T, Nolan GP. Episomal vectors rapidly and stably produce high-titer recombinant retrovirus. Hum Gene Ther. 1996; 7:1405–1413. [PubMed: 8844199]

20. Steff AM, Fortin M, Arguin C, Hugo P. Detection of a decrease in green fluorescent protein fluorescence for the monitoring of cell death: an assay amenable to high-throughput screening technologies. Cytometry. 2001; 45:237–243. [PubMed: 11746092]

21. Mitsiades CS, Mitsiades NS, Bronson RT, et al. Fluorescence imaging of multiple myeloma cells in a clinically relevant SCID/NOD *in vivo* model: biologic and clinical implications. Cancer Res. 2003; 63:6689–6696. [PubMed: 14583463]

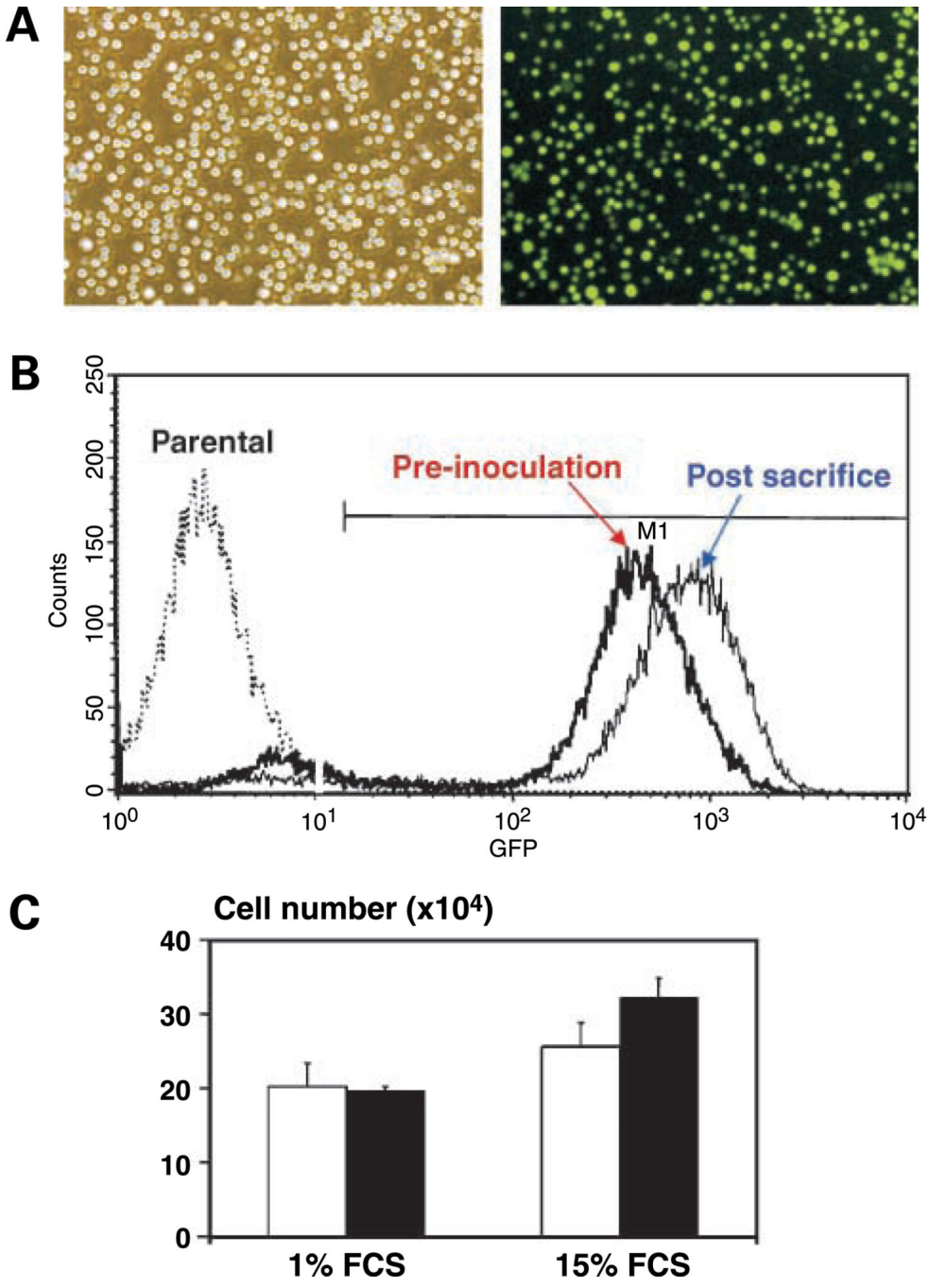

Figure 1.

Stable high-level expression of eGFP in murine 5TGM1 myeloma cells *in vitro* and *in vivo*. **A**, phase-contrast (*left*) and fluorescence (*right*) photomicrographs of stable eGFP-expressing 5TGM1 transductants (5TGM1-eGFP H1.1+) *in vitro* (*top*). **B**, flow cytometric analysis of eGFP H1.1+ cells showing stable high-level expression of GFP in 5TGM1 myeloma cells *in vivo*. On day 28 post tumor cell inoculations, bone marrow was flushed from long bones of the lower limbs of myeloma-bearing mouse and analyzed by single-channel flow cytometry. There was no significant difference in the median fluorescence of

genetically engineered 5TGM1-eGFP cells preinoculation and those harvested post-sacrifice [*Y axis*, number of cells per channel; *X axis*, relative fluorescence intensity in arbitrary units (on a log scale)]. eGFP H1.1+ cells have now been maintained in culture for > 12 mo continuously without drift/loss of GFP expression. Repeated freezing and thawing also has no effect on GFP expression (data not shown). **C**, there is no significant difference in growth between parental 5TGM1 cells (**open columns**) and 5TGM1-eGFP H1.1+ cells (*solid columns*). Cells were plated in standard media supplemented with high (15%) or low (1%) serum and viable cells (determined by trypan blue dye exclusion) were enumerated after 24 h.

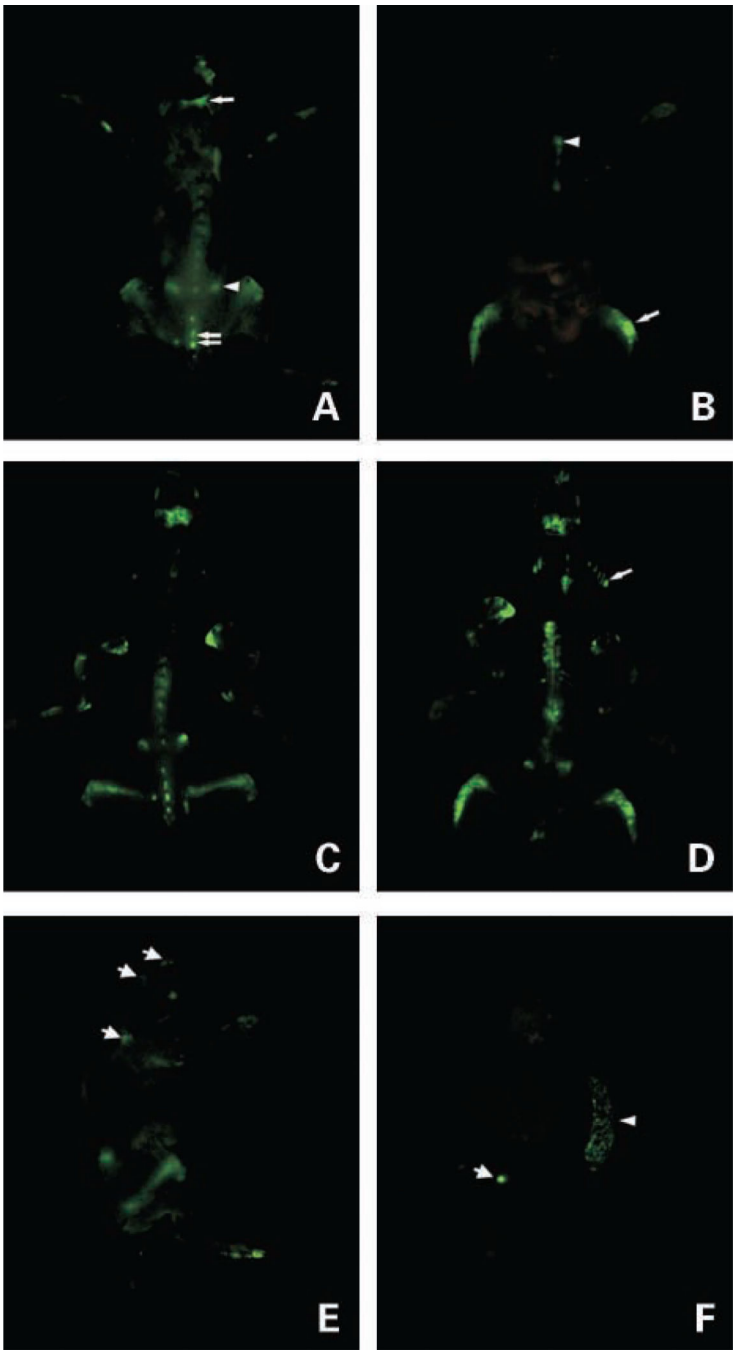

Figure 2.

Whole-body optical images of eGFP-expressing myeloma tumors in skeleton of a live intact mouse. **A** and **B**, whole-body, high-resolution fluorescence images of dorsal and ventral views, respectively, of a live myeloma tumor – bearing mouse 4 wks after i.v. inoculation of 10^6 5TGM1-eGFP cells. **A**, *single arrow*, calvaria; *arrowhead*, iliac crest; *double arrows*, spine. **B**, *arrowhead*, sternum; *arrow*, hind limb. **C** and **D**, corresponding fluorescence images of the exposed skeleton of the same mouse. **D**, *arrow*, ribs. **E**, whole-body fluorescence image of left lateral view of the same mouse. Apart from clearly visible tumors

in the femora and iliac crest tumors, fluorescent tumors are also visible in the base of the skull and scapula (*arrows*). Note the autoflourescent toenails. **F**, fluorescence image of visceral organs (spleen, brain, liver, kidneys, ovaries, heart and lungs, and adrenal glands) of the same mouse showing tumor infiltration of the spleen (*arrowhead*) and tumor in one of the ovaries (*arrow*); all the other organs were tumor-free.

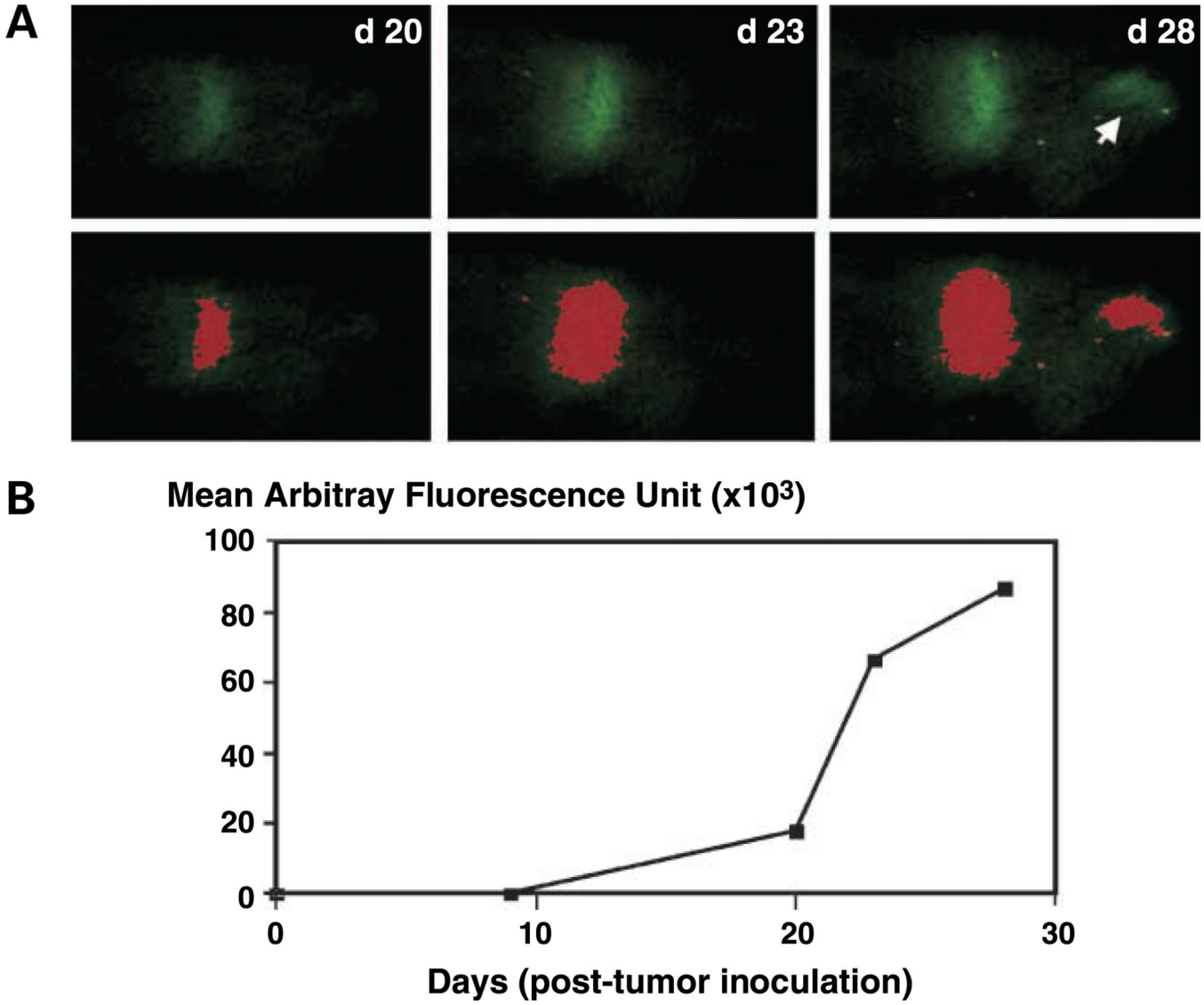

Figure 3.

Real-time fluorescence monitoring of tumor growth *in situ* in individual bones of tumor-bearing mice. **A**, series of dorsal external fluorescence images of foci of myeloma tumors in calvaria of a 5TGM1-eGFP myeloma – bearing mouse from day 20 through day 28 post tumor cell inoculation (*top*). All images were acquired in identical fashion. Note the appearance of a second tumor focus between day 23 and day 28 post inoculation (*arrow*). No fluorescence was detected at baseline or at any time point before day 20 even after prolonged exposure of up to 60 s. For each time point, a computer-rendered digitized image of area of fluorescence was generated as described in Materials and Methods (*bottom*). Note that the threshold set allowed inclusion of a new tumor focus that appeared between day 23 and day 28 post inoculation. **B**, tumor growth curve determined from computerized analysis of serial images acquired as in (**A**) showing a time-dependent tumor progression.

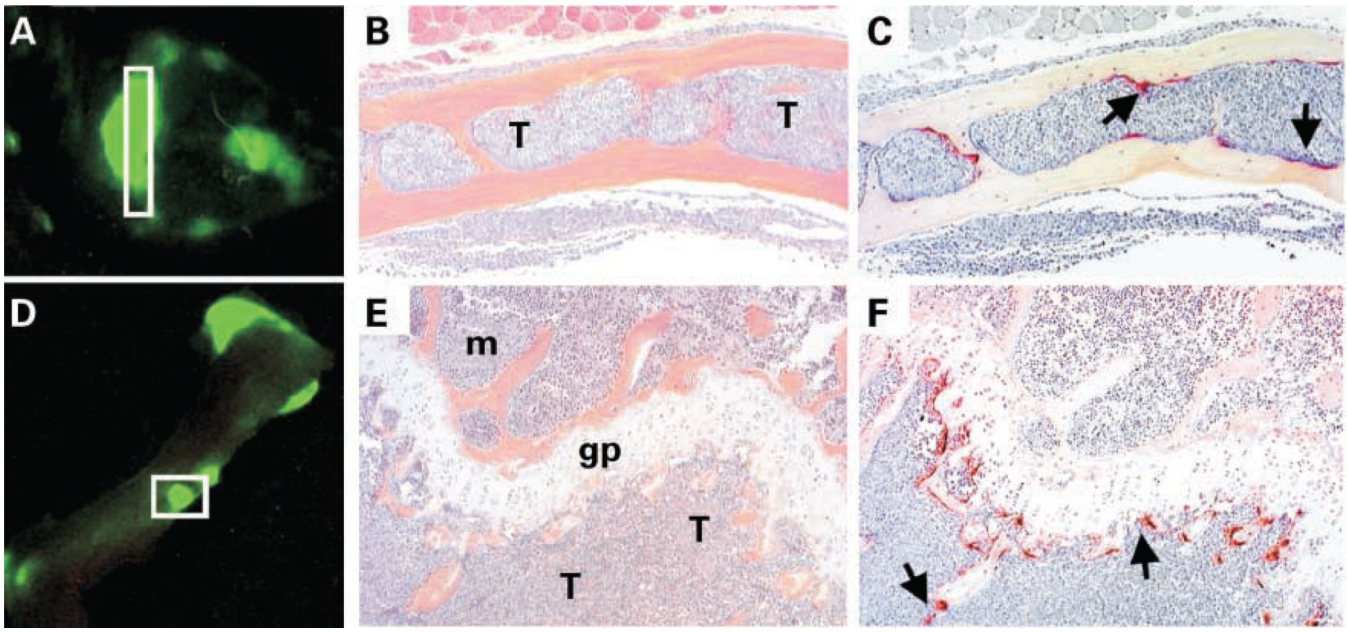

Figure 4.

Increased osteoclast activity associated with eGFP-expressing myeloma tumor cells in two different types of bone *in vivo*. **A – C**, skull; **D – F**, scapula/humerus. **A** and **D**, optical images of fluorescent tumor foci in skull and humerus, respectively, of a myeloma-bearing mouse obtained on day 28 post tumor cell inoculation. **B** and **E**, representative photomicrographs of sections through *insets* in (**A**) and (**D**) stained with H&E. **C** and **F**, serial sections stained for tartarate-resistant acid phosphatase activity (*red stain*) to reveal osteoclasts. The medullary cavity of the calvaria is completely infiltrated by tumor (**B**) and several osteoclasts (*arrows*) can be seen lining the interface between the endosteal surface of bone and tumor cells (**C**). There is also complete tumor infiltration of metaphysis of the humerus (**E**) associated with a marked increase number of osteoclasts (*arrows*; **F**). Note the absence of osteoclasts on the opposing side of the growth plate where normal marrow has not been replaced by tumor. *T*, tumor; *m*, normal marrow; *gp*, growth plate.

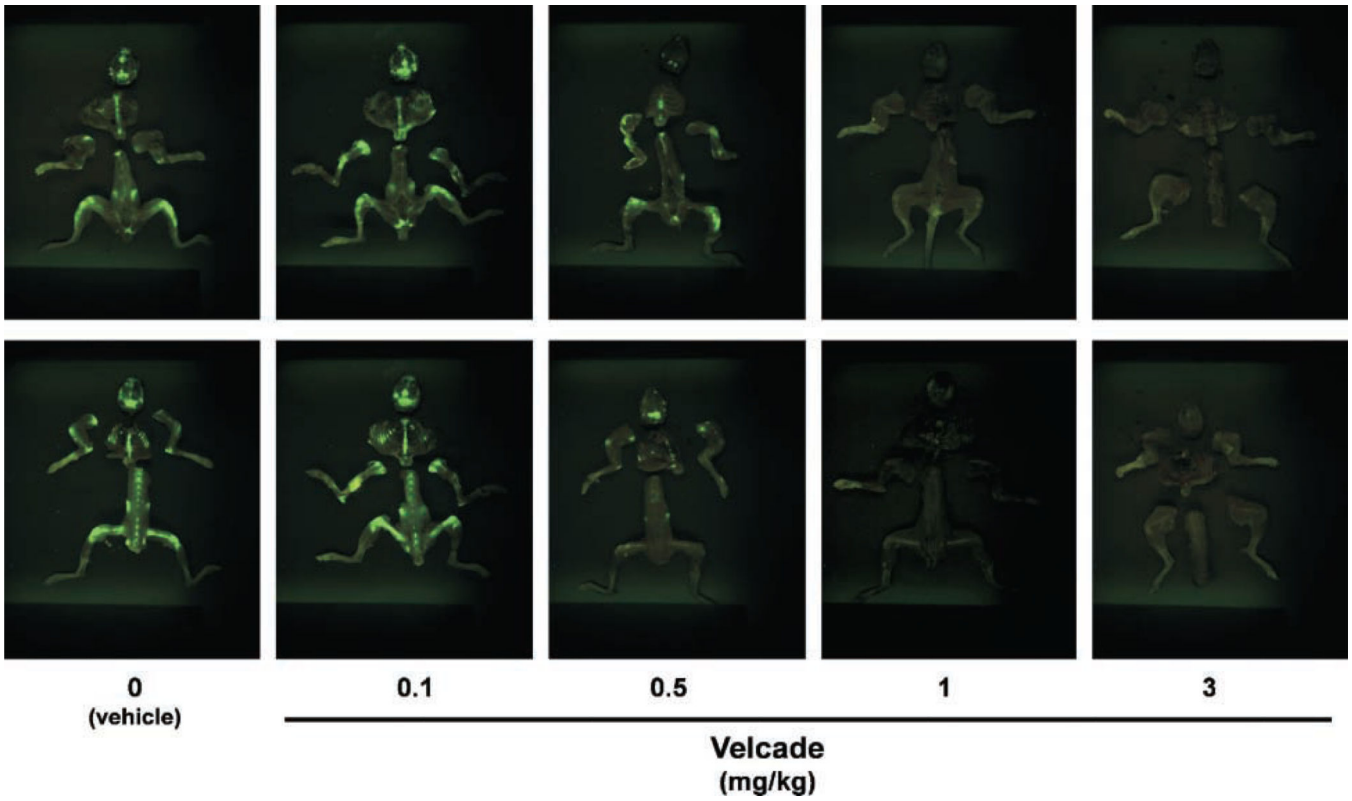

Figure 5.

Antitumor efficacy of Velcade shown by GFP imaging of 5TGM1-eGFP myeloma – bearing mice. Myeloma-bearing mice were randomized to receive Velcade or vehicle i.p. for 4 wks, after which they were sacrificed and the freshly isolated skeletons imaged as described in Materials and Methods. Fluorescence images of bones of a representative mouse from each group. *Top*, anteroposterior view; *bottom*, posteroanterior view. Note the dose-dependent effect of Velcade and the almost complete absence of tumor foci (*green fluorescence*) in the mice that received the two highest doses of the drug.

Table 1

Antitumor effect of Velcade in 5TGM1-eGFP myeloma–bearing mice determined by GFP imaging

Velcade (mg/kg)	Calvariae	Pelves, scapulae, and limbs	Rib cages	Spines	Spleens	Soft tissues
0	100	100	100	100	75	100
0.1	100	100	100	88	75	75
0.5	63	75	50	38	0	38
1*	57	14	29	0	0	43
3†	0	0	0	0	0	0

NOTE: Mice (n = 8 per group) inoculated with 5TGM1-eGFP myeloma cells were treated with or without Velcade at the doses indicated by i.p. injection thrice a week for 4 wks. Immediately after sacrifice, tissues were optically imaged in anteroposterior and posteroanterior orientations as described in Materials and Methods. Data presented represent the percentage of mice in each group with one or more fluorescent foci in both orientations.

*One mouse in this group died a few days before the end of the experiment.

†One tumor-bearing mouse in this 3 mg/kg group and one non – tumor-bearing mouse in the control group also receiving 3 mg/kg Velcade died a few days after the start of the experiment (due to toxicity), and thus dose administered was reduced thereafter to 2 mg/kg.